Chromatic dispersion-free diffraction grating based single-shot autocorrelator

Shunxing Tang[1] · Xiuqing Jiang[1] · Yajing Guo[1] · Li Zhou[1] · Lin Yang[1] · Baoqiang Zhu[1] · Jianqiang Zhu[1]

Abstract

A chromatic dispersion-free diffraction-grating single-shot autocorrelator (grating-SSA) is proposed. The grating-SSA is described theoretically, and its performance is experimentally characterized. The results demonstrate that the SSA measurement range can be expanded as expected, and the measurement accuracy is the same as that of a conventional SSA. The measurement range of an optimized design can be expanded to almost three times as wide as that of the same size BBO-based conventional SSA, achieving a 100 ps measurement range for an 30 mm diameter non-linear crystal.

1 Introduction

Ultrafast lasers have been widely applied in recent years. Two of the most important parameters of ultrafast lasers are pulse-width and pulse contrast. Short pulse cannot be measured directly, unlike long pulses, which can be measured by oscilloscope or streak-camera. Oscilloscopes only yield the intensity and do not provide any information on the phase of the pulse. Thus, various indirect measurement methods have been proposed over the past few decades, such as the autocorrelator, frequency-resolved optical gating (FROG), spectral phase interferometry for direct electric field reconstruction (SPIDER), etc. [1–11]. Autocorrelators can only provide some information on the approximate temporal intensity, however, pulse measurement techniques such as FROG and SPIDER yield full temporal information of the field i.e. the intensity and phase. Generally, these methods employ non-linear crystals to generate indirect signals, thus, the measurement range is limited by crystal size and single shot measurement configuration. Considering the single shot autocorrelator (SSA) for example, the measurement range is $D\sin\phi/2c$, where D is the diameter of crystal, ϕ is the angle between the two arms, and c is the speed of light in vacuum. To increase the measurement range of SSAs, Saltiel and Stankov [12] proposed a diffraction grating autocorrelator,

and a similar scheme has been applied in FROG [13, 14]. However, the grating dispersion induces measurement error, limiting applicability to wavelength ranges narrow enough to meet the measurement accuracy requirements [15–17].

2 Chromatic dispersion compensation for tilted pulse front

Figure 1 shows the layout of a type of chromatic dispersion compensator for a tilted pulse front. The first-order diffracted light of a short pulse from a reflection grating (referred to as Grating-1) is transmitted to an Offner triplet, and the output beam, referred to as the pre-compensation beam here, is diffracted again by the same grating. The first-order diffraction beam, with chromatic dispersion both parallel and orthogonal to the propagation axis, is diffracted by a second grating (referred to as Grating-2), which is parallel to Grating-1. The first-order diffraction light of the pre-compensation beam from Grating-2 is transmitted to a special working plane, at which the beam has neither temporal or spatial chromatic dispersion. The working plane must be parallel to Grating-2, and the distance between Grating-2 and the working plane should be twice the distance between Grating-1 and the co-center of the Offner triplet. Suppose the size of the beam incident on Grating-1 is small enough to be considered as a line, that includes rays of all the wavelengths of the short pulse, and the first order diffraction ray of wavelength λ_0 is perpendicular to the surface of Grating-1. The rays will be incident on the Grating-1 again after the Offner triplet, and the position of each ray (wavelength λ) will be dispersed

✉ Xiuqing Jiang
jiangxiuqing1991@163.com

1   National Laboratory on High Power Laser and Physics, Shanghai Institute of Optics and Fine Mechanics, Chinese Academy of Sciences, Shanghai 201800, China
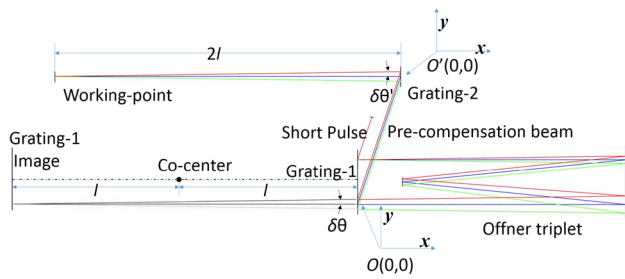
Fig. 1 Layout of diffraction grating SSA

Fig. 2 Layout of generated chromatic dispersion-free tilted pulse front

because of the dispersion of the grating. The dispersion can be written as [18]:

$$\delta y/\delta \lambda = 2l/[d_1 \cos^3 \theta(\lambda)], \tag{1}$$

where δy is the laser ray location on Grating-1 between wavelength λ and λ_0, l is the distance between Grating-1 and the co-center of the Offner triplet, d_1 is the grating constant of Grating-1, $\theta(\lambda)$ is the diffraction angle of the incident beam for Grating-1, which can be written as:

$$\theta(\lambda) = \arcsin(\lambda/d_1 - \sin\alpha), \tag{2}$$

where α is the angle of incidence of the short pulse on Grating-1, and it is also the angle of incidence of the pre-compensation beam on Grating-2. Defining new coordinates (Cartesian), the origin of which is located at the point where the ray λ_0 meets Grating-2, the function of the first-order diffraction rays of the pre-compensation beam can be written as:

$$y = \delta y + \tan[(\delta\theta'(\lambda))]x, \tag{3}$$

where $\delta\theta'(\lambda)$ is the diffraction angle difference between wavelength λ and λ_0, and $\theta'(\lambda)$ is the diffraction angle of the incident beam for Grating-2, , which can be written as:

$$\theta'(\lambda) = \arcsin(\lambda/d_2 - \sin\alpha), \tag{4}$$

where d_2 is the grating constant of Grating-2. Suppose $d_2 = d_1 = d$, from Eqs. (2) to (4):

$$\tan(\delta\theta') = \tan(\delta\theta) = \delta\lambda/[d\cos^3\theta] \tag{5}$$

where $\delta\lambda = \lambda - \lambda_0$. From Eqs. (1) and (5):

$$y = (2l + x)\delta\lambda/[d\cos^3\theta]. \tag{6}$$

Each of the rays will pass through the working point $(-2l, 0)$, thus, the spatial dispersion has been reduced. As the distance between the working point and Grating-2 equals the distance between Grating-1 and the Grating-1 image, and the parallel pair of gratings do not introduce additional optical path aberration, according to Fermat's principle, there is no temporal dispersion at the working point.

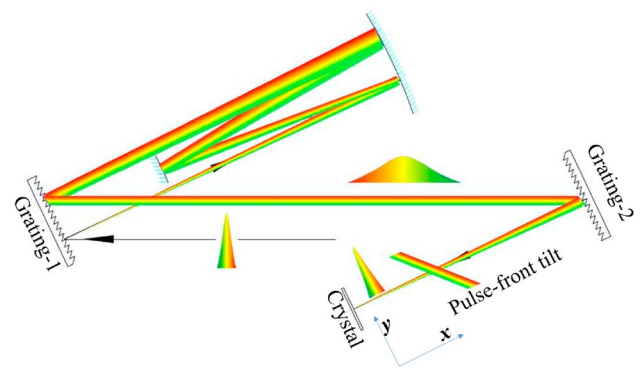As shown in Fig. 2, placing a nonlinear crystal at the working point, the pulse-front will be tilted by Grating-2 without temporal dispersion or spatial dispersion. This is useful for the SSA, or can be used in FROG, as well as in single shot pulse contrast measurements.

3 Performance of the chromatic dispersion-free grating-SSA

An experiment was conducted to compare the performance of the chromatic-dispersion-free grating-SSA with a conventional SSA, the configuration is shown in Fig. 3. As a conventional SSA, the pulse is split into two beams by a fifty-fifty beam splitter BS. One of the beams is directed upwards, referred to as the up-arm, reflected by mirrors M1 and M2, and is incident on the BBO crystal at an angle γ. The incidence planes of mirrors M1 and M2 should be perpendicular to each other. The other beam passes through the BS, referred to as the down-arm, is reflected by mirrors M3 and M4, and is incident on the BBO crystal at an angle $-\gamma$. The incidence planes of the beam-splitter BS and mirror M3 should be perpendicular to each other, and the incidence planes of mirrors M3 and M4 should be perpendicular to each other as the same. The optical-path lengths between the BS to the BBO crystal of the two arms should be carefully adjusted to be equal. As a grating-SSA, the input beam is replaced by a chromatic dispersion-compensated
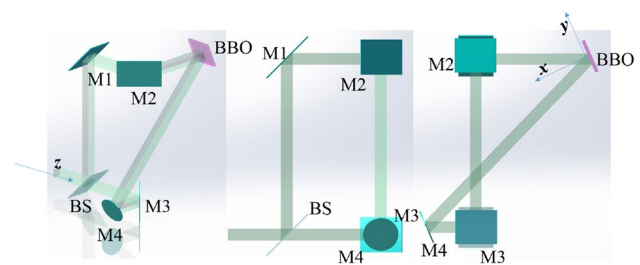

Fig. 3 Configuration for comparison of SSAs. (M1–4: mirrors; BBO: β-BaB$_2$O$_4$ crystal; BS: beam splitter)

tilted pulse-front beam based on the configuration shown in Fig. 2, and the optical-path between the BBO crystal and the Grating-1 should satisfy the relations described in the previous section. Parameters used in the experiment, were center wavelength $\lambda_0 = 1.03\ \mu m$, grating constant $d = 1/600$ mm, and as shown in Fig. 4, the tilt angle of pulse front is calculated as:

$$u = \arctan(\lambda_0/d). \tag{7}$$

Functions to define the plane for the tilted pulse-front of each arm can be written as,

$$z + x/\tan(\gamma) + y\tan(u)/\sin(\gamma) = 0, \tag{8a}$$

$$-z + x/\tan(\gamma) - y\tan(u)/\sin(\gamma) = 0, \tag{8b}$$

where γ is the incident angle of each beam. As shown in Fig. 4, the intersection line of the two planes is written as,

$$\begin{cases} z = -(\tan u/\sin\gamma)y \\ x = 0 \end{cases}, \tag{9}$$

if the arm descript by Eq. (8a) adds a temporal delay δt, the arm can be re-written as,

$$z - c\delta t\sin\gamma + (x - c\delta t\cos\gamma)/\tan(\gamma) + y\tan(u)/\sin(\gamma) = 0, \tag{10}$$

where c is the speed of light in air. The intersection line of the two planes becomes,

$$\begin{cases} z = -(\tan u/\sin\gamma)y + c\delta t/2\sin\gamma \\ x = -c\delta t/2\sin\gamma \end{cases}. \tag{11}$$

Projecting the lines described by Eqs. (9) and (11) to the *YZ* plane, the distance between which is,

Fig. 4 Intersection of arms showing the tilt angle of the pulse-front, u

$$\Delta = c\delta t/[2\sin\gamma\sqrt{1 + (\tan u/\sin\gamma)^2}]. \tag{12}$$

The SSA signal is always generated at the center of the non-linear crystal, thus the measurement range should be written as,

$$\delta t = D\sin\gamma\sqrt{1 + (\tan u/\sin\gamma)^2}/c, \tag{13}$$

where D is the diameter of the crystal. without pulse-front tilt, or for the conventional SSA, $u = 0$, thus,

$$\delta t = D\sin\gamma/c. \tag{14}$$

For the same configuration, the grating-based SSA measurement range is $\sqrt{1 + (\tan u/\sin\gamma)^2}$ times that of the conventional SSA. Substituting the values of γ, λ_0, d, into Eqs. (13) and (14), the calculated measurement range of the proposed SSA is 1.9 times that of the conventional SSA.

To calibrate the system, a 2 mm thick fused silica plate is inserted into one of the arms to produce a 3 ps time delay, shifting the SSA signal at the camera. This yields a coefficient representing the ratio of the real pulse width to the SSA signal width in units of pixels. Figure 5 shows the calibration results for the conventional SSA and grating SSA, and yields 35.7 fs/pixel and 68.2 fs/pixel, respectively. The observed measurement range of the grating based SSA is 1.9 times that of the conventional SSA, which agrees with the theoretical analysis above. Measurements results are shown in Table 1 for pulse widths of 0.26 ps, 1 ps, 2 ps, 3 ps, and 5 ps, respectively.

The nominal pulse widths are provided by the manufacturer, and the SSA signal is affected by the beam profile [19]. The results of SSA measurements would be more precise if the beam profile was considered when analyzing the results.

4 Discussion

Rewriting Eq. (13) we obtain,

$$\delta t = D\sqrt{(\sin\gamma)^2 + (\tan u)^2}/c, \tag{15}$$

To design a large measurement range SSA, we should increase the size of non-linear crystal, D, or increase the incident angle of each beam, γ, to the limit of the acceptable angle of second harmonic generation (SHG), or increase the pulse front tilt angle, u, to the limit of 45°. To design a 100 ps-range dispersion-free SSA, if we use BBO for SHG, the maximum value of γ is 22.5°, and the corresponding diameter of the BBO crystal is 28mm, while if we use lithium triborate (LBO) for SHG, the maximum value of γ is 10.5°, and the corresponding diameter of the crystal is 29.5 mm. This size of LBO is not hard to obtain refers to the same size BBO. According to Eq. (14), to design a conventional SSA by the BBO crystal mentioned above, the measurement range is 35.7 ps, which is 1/2.8 times that of 100 ps.
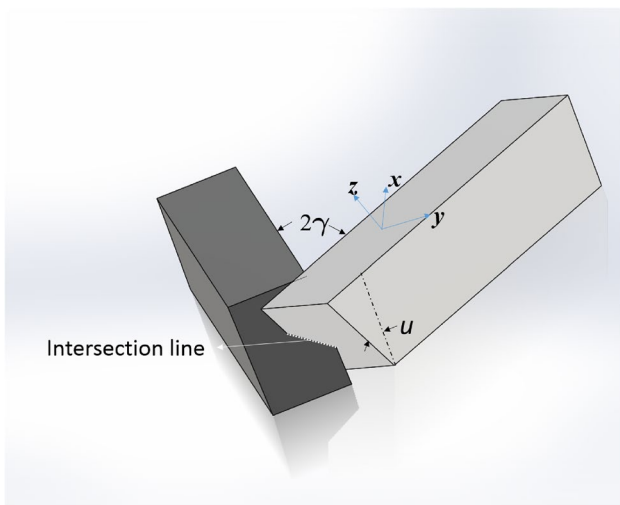
Fig. 5 SSA calibration for conventional (left) and grating (right) SSAs

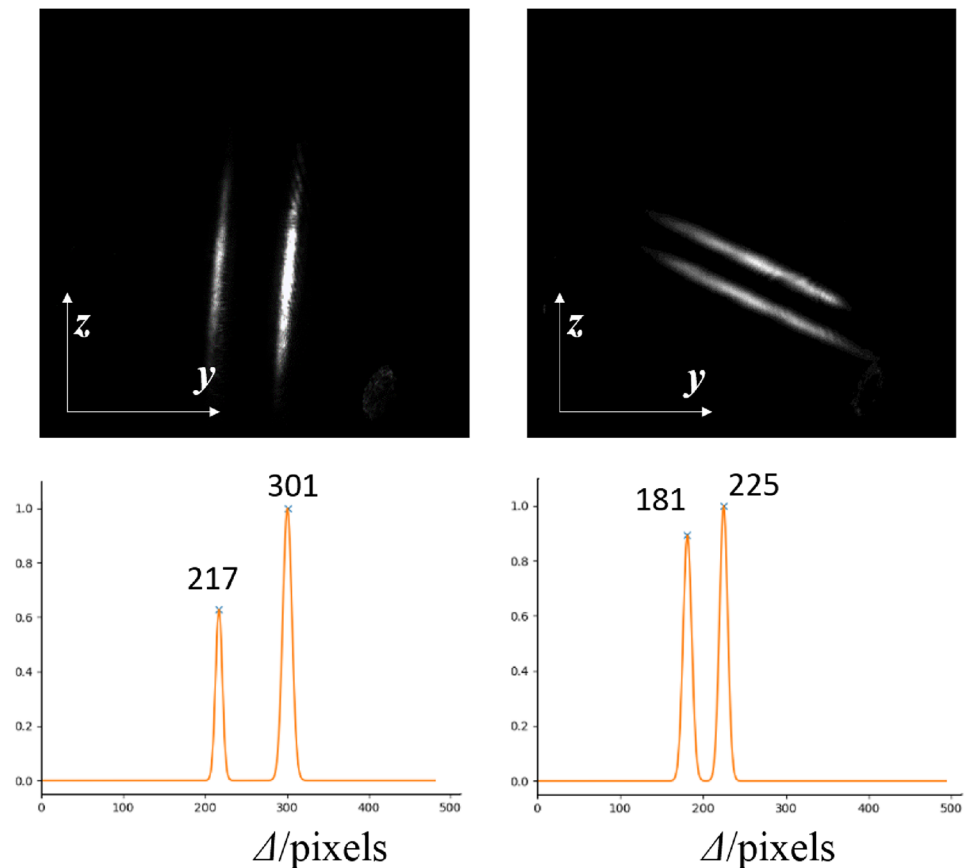**Table 1** Conventional and grating SSA measured pulse widths

Nominal pulse width/ps	Conventional SSA/ps	Grating SSA/ps
0.26	0.23	0.25
1	0.95	0.62
2	1.86	1.54
3	2.6	2.7
5	3.49	4.86

5 Conclusion

A chromatic dispersion-free diffraction-grating single-shot autocorrelator (grating-SSA) is proposed. We describe it theoretically, and evaluate the performance experimentally by comparison with a conventional SSA. The results demonstrate that the measurement range of an SSA can be increased as expected, and that the measurement accuracy is the same as that of a conventional SSA. The measurement range of an optimized design can be expanded to almost 2.8 times that of a conventional BBO crystal SSA, or 100 ps measurement range for a 30 mm diameter nonlinear crystal.

References

1. R.N. Gyuzalian, S.B. Sogomonian, Z. Gy, Opt. Commun. **29**, 239–242 (1979)
2. F. Salin, P. Georges, G. Roger, A. Brun, Appl. Opt. **26**, 4528–4531 (1987)
3. R. Trebino, D.J. Kane, J. Opt. Soc. Am. A **10**, 1101–1111 (1993)
4. R. Trebino, D.J. Kane, Opt. Lett. **18**, 823–825 (1993)
5. D.J. Kane, R. Trebino, IEEE J. Quantum Electron. **29**, 571–579 (1993)
6. R. Trebino, *Frequency-Resolved Optical Gating: The Measurement of Ultrashort Laser Pulses* (Springer, Boston, 2002)
7. C. Iaconis, I.A. Walmsley, Opt. Lett. **23**, 792–794 (1998)
8. C. Iaconis, I.A. Walmsley, IEEE J. Quantum Electron. **35**, 501–509 (1999)
9. P. O'Shea, M. Kimmel, X. Gu, R. Trebino, Opt. Lett. **26**, 932–934 (2001)
10. C. Zhou, E. Dai, G. Li, Opt. Express **13**, 6145 (2005)
11. J. Ma, P. Yuan, J. Wang, G. Xie, H. Zhu, L. Qian, High Power Laser Sci. Eng. **6**(4), e61 (2018)
12. S.M. Saltiel, K.A. Stankov, Appl. Phys. B **35**, 45–48 (1984)
13. K. Oba, X. Zhang, P.C. Sun, Y. Mazurenko, Y. Fainman, Proc. SPIE **3466**, 185–195 (1998)

14. I. Jovanovic, C. Brown, C. Haefner, et al., in *Quantum Electronics and Laser Science Conference* (Optical Society of America, 2007) (p. JThD137).
15. S.M. Saltiel, K.A. Stankov, P.D. Yankov, L.I. Telegin, Appl. Phys. B **40**, 25–27 (1986)
16. S. Tang, L. Yang, X. Jiang, Y. Guo, B. Zhu., in *The 3rd International Symposium on HPLSE, Suzhou, Jiangsu, April 9–13* (2018)
17. G. Figueira, L. Cardoso, N. Lopes, J. Wemans, J. Opt. Soc. Am. B **22**, 2709–2714 (2005)
18. X. Zhang, Z. Xu, X. Wang, Chin. J. Lasers **29**(2), 127–130 (2002)
19. X. Kong, S. Yan, J. Yu, D. Liu, X. Ouyang, B. Zhu, J. Zhu, Chin. J. Lasers **44**(11), 1104001 (2017)